Journal of Applied Mathematics & Bioinformatics, vol. x, no. x, 2011, x-x
ISSN: 1792-6602(print), 1792-6939(online)

Hybrid regularization for wavelet frame and total variation with application to Poisson noise removal

Xiaojuan Yang [1]

Abstract

Blurred images corrupted by Poisson noise frequently appear in various applications such as medical and astronomical imaging. Due to the strong edge preserving ability, the Total variation (TV) regularization has been developed as an important regularization method to solve the Poisson denoising problem. However, TV introduces staircase effects. In this paper, we propose a hybrid variational model which takes advantages of the wavelet tight frame and TV. An efficient iterative algorithm based on the augmented Lagrangian technique is proposed. Under some conditions, the convergence property of the proposed algorithm is also investigated. Numerical experiments illustrate the effectiveness of the proposed method.

Mathematics Subject Classification : 68U10, 65K10, 90C25, 62H35
Keywords: Total variation, Poisson noise, wavelet tight frame, regularization

1 Introduction

The deblurring problem for images corrupted by Poisson noise is an important task in various applications, such as astronomical [1], medical [2] and pho-

[1]School of Mathematical Sciences, Nanjing Normal University, Taizhou College Taizhou, 225300, P. R. China. e-mail: yxjwyz@163.com

Article Info: *Received* : January 10, 2011. *Published online* : July 17, 2011

tographic imaging [3]. The problem of restoration of Poissonian images has received considerable attention in recent years. Image restoration in such fields of applications can often be formulated as linear ill-posed problems. The goal of image deblurring and denoising is to recover approximate images of original images from blurred and noisy measurements.

Let $u \in \mathbb{R}^{n\times n}$ be the original image, $f \in \mathbb{R}^{n\times n}$ be the observed image, $K : \mathbb{R}^{n\times n} \to \mathbb{R}^{n\times n}$ is a blurring operator which model a convolution or some other linear observation mechanism, such as emission tomography. Then the degradation model can be written as

$$f = \mathcal{P}(Ku + b), \tag{1}$$

where $\mathcal{P}(\alpha)$ denotes a Poisson distributed random vector with mean α, and $b \geq 0$ is an array describing the expected value of the background emission.

We know that the intensity $f_{i,j}$ in the pixel (i, j) is a random variable that follows a Poisson law of mean $(Ku + b)_{i,j}$. The likelihood probability distribution of (1) can be expressed as

$$p(f|Ku) = \prod_{i,j=1}^{n} \frac{[(Ku + b)_{i,j}]^{f_{i,j}}}{f_{i,j}!} e^{-(Ku+b)_{i,j}}. \tag{2}$$

By taking the negative logarithms of the likelihood and adding a suitable constant leads to the log-likelihood function [1, 4]

$$-\log[p(f|Ku)] = \sum_{i,j=1}^{n} \Big\{ f_{i,j} \log \frac{f_{i,j}}{(Ku + b)_{i,j}} + (Ku + b)_{i,j} - f_{i,j} \Big\},$$

By dropping some terms independent of u, the above equation is equivalent to

$$-\log[p(f|Ku)] = \sum_{i,j=1}^{n} (Ku + b)_{i,j} - f_{i,j} \log(Ku + b)_{i,j}, \tag{3}$$

the unknown image can be recovered by minimizing the likelihood function (3) with respect to u.

The standard algorithm for the minimization of (3) is the Richardson-Lucy (RL) algorithm [5, 6], which takes account Poisson statistics of the photon counting. The algorithm has non-negativity of the iterates and flux conservation (in the case $b = 0$). However, this method is unable to prevent noise

amplification sufficiently during the iterative process due to the ill-posedness of the inverse problem.

Since as a consequence of noise and ill-posedness of the inverse problem, in general the minimizers of the function $-\log[p(f|Ku)]$ are not reliable solutions of the image restoration problem and they are sparse [7, 8, 9]. Usually, some regularity condition has to be imposed on the solution space in order to turn the underlying ill-posed problem to a well-posed one [10]. The minimization of the function $-\log[p(f|Ku)]$ is replaced by the minimization of a penalized function of the form

$$\min_u \sum_{i,j=1}^{n} (Ku+b)_{i,j} - f_{i,j}\log(Ku+b)_{i,j} + \mu\Phi_{reg}(u), \tag{4}$$

where $\Phi_{reg}(u)$ is the regularizer that enforces the a priori knowledge and the regularization parameter μ is used to balance the two terms.

The Tikhonov-like class [11] regularization, which includes $\Phi_{reg}(u) = \|Lu\|_2^2$, is a standard regularization method. The matrix L is the identity operator or differentiation operator. The authors [12, 13] proposed an efficient hybrid gradient projection-reduced Newton method for the problem of restoration of Poissonian images with Tikhonov regularizater. In spite of the computational advantages, the Tikhonov regularization tend to make images overly smooth, so they often fail to adequately preserve important image attributes such as sharp edges.

Another well-known class of regularizers is Total variation (TV), which was proposed for image denoising by Rudin, Osher and Fatemi in [14], and then extended to image deblurring in [15]. TV regularizer restricts the domain of possible candidate solutions to those having sparse gradient, i.e. the solution of (4) for which $\|u\|_{TV}$ is minimal, where

$$\|u\|_{TV} \triangleq \|\nabla u\|_1 = \sum_{1\le j,k\le n} \sqrt{|(\nabla u)^x_{j,k})|^2 + |(\nabla u)^y_{j,k})|^2}, \tag{5}$$

is the discrete total variation of u. The discrete gradient operator $\nabla : \mathbb{R}^{n\times n} \to (\mathbb{R}^{n\times n}, \mathbb{R}^{n\times n})$ with periodic boundary condition is defined by

$$(\nabla u)_{j,k} = ((\nabla u)^x_{j,k}, (\nabla u)^y_{j,k})$$

with

$$(\nabla u)^x_{j,k} = \begin{cases} u_{j+1,k} - u_{j,k} & \text{if } 1 \le j < n, \\ u_{j,1} - u_{j,n} & \text{if } j = n, \end{cases}$$

$$(\nabla u)^y_{j,k} = \begin{cases} u_{j,k+1} - u_{j,k} & \text{if } 1 \leq k < n, \\ u_{1,k} - u_{n,k} & \text{if } k = n, \end{cases}$$

for $j, k = 1, \cdots, n$. Here $u_{j,k}$ refers to the (j, k) pixel location of the image.

Various algorithms were proposed to solve (4) with $\Phi_{reg}(u) = \|u\|_{TV}$. Sawatzky et al. [16] proposed EM-TV algorithm. Based on EM-TV algorithm, Brune et al.[18] proposed primal and dual Bregman-EM-TV algorithms. In [34], Figueiredo et al. used the alternating direction method of multipliers (ADMM) method to restore Poissonian images with the TV function, and they present sufficient conditions for existence and uniqueness of solutions.

While preserving sharp discontinuities, the TV-based regularization cannot preserve details and textures very well in regions with complex structures because of the staircase effects [19]. To mitigate this problem, one approach [23] reducing the staircase effect is adding a higher order regularization term to the original ROF model. The other is based on wavelet frames. It is well known that images, especially natural images, can be regarded as piecewise smooth functions, and wavelet frames can usually provide good sparse approximations to piecewise smooth functions. The ability to approximate images sparsely is an important characteristic of wavelets, see [22]. There are mainly three formulations utilizing the sparseness of the wavelet frame coefficients, namely analysis based approach, synthesis based approach, and balanced approach. In our work, we will focus on the analysis approach because it provides a direct link to the local geometry of u [29]. The analysis approach is often modeled as a regularization term as follows

$$\Phi_{reg}(u) = \|Wu\|_1,$$

where W is the analysis operator and Wu is the corresponding wavelet frame coefficients.

Framelet-based algorithms are introduced in [34, 21, 20] for Poissonian image restoration. However, the methods implemented by pure wavelet thresholding also revoke unpleasant artifacts around discontinuities as a result of Gibbs phenomenon.

In this paper, in order to combine the advantages of wavelet-based and total variation methods and avoid their main drawbacks, we proposed the following

hybrid variation model

$$\min_u \sum_{i,j=1}^{n} (Ku+b)_{i,j} - f_{i,j}\log(Ku+b)_{i,j} + \alpha\|Wu\|_1 + \beta\|\nabla u\|_1 \qquad (6)$$

for Poissonian image restoration. The proposed method can reduce the staircase effect and remove the Gibbs oscillations in the restored images.

This paper is organized as follows. In Section 2, we give some preliminaries of framelets and examples of framelets used in this paper. In Section 3, we employ the ADMM for the modle (6), and discuss the convergence of the algorithm. Some numerical experiments are given to illustrate the performance of the proposed algorithm in Section 4.

2 Framelets

In this section, we present some preliminaries of tight framelets. For simplicity, we only present the univariate framelets and the framelets for two variables can be constructed by tensor product of univariate framelets. The details about how to construct the tight framelets and the detailed frame theory can be found in [24, 25].

A system $X \subset L_2(\mathbb{R})$ is called a tight frame of $L_2(\mathbb{R})$ if

$$f = \sum_{g\in X} < f, g > g, \quad \forall f \in L_2(\mathbb{R}). \qquad (7)$$

This is equivalent to

$$\|f\|_2^2 = \sum_{g\in X} | < f, g > |^2 \quad \forall f \in L_2(\mathbb{R}), \qquad (8)$$

where $< \cdot, \cdot >$ and $\|\cdot\|_2 =< \cdot, \cdot >^{\frac{1}{2}}$ are the inner product and norm of $L_2(\mathbb{R})$. We can see that an orthonormal basis is a tight frame, since the identities (7) and (8) hold for arbitrary orthonormal bases in $L_2(\mathbb{R})$. Hence, tight frames are generalization of orthonormal bases that bring in the redundancy which is often useful in applications such as denoising, see, e.g., [26].

For given $\Psi := \{\psi_1, \cdots, \psi_q\} \subset L_2(\mathbb{R})$, the corresponding wavelet (or affine) system $X(\Psi)$ generated by Ψ is defined by the collection of dilations and shifts of Ψ as

$$X(\Psi) = \{2^{k/2}\psi_l(2^k x - j) : 1 \le l \le q; k, j \in Z\}.$$

When $X(\Psi)$ forms a tight frame of $L_2(\mathbb{R})$, each function $\psi_l, l = 1, \cdots, q$, is called a (tight) framelet and the whole $X(\Psi)$ is called a tight wavelet frame.

The construction of framelet Ψ, which are desirably (anti)symmetric and compactly supported functions, are usually based on a multiresolution analysis (MRA) that is generated by some refinable function ϕ with refinement mask a_0 satisfying the refinement equation

$$\hat{\phi}(2\cdot) = \hat{a}_0\hat{\phi}(\cdot),$$

where $\hat{\phi}$ is the Fourier transform of Ψ, and $\hat{a}_0$ which is 2π periodic is the Fourier transform of a_0. The idea of an MRA-based construction of framelet Ψ is to find masks a_l, which are finite sequence, such that

$$\hat{\psi}_l(2\cdot) = \hat{a}_l\hat{\phi}(\cdot), \quad l = 1, \cdots, q,$$

where $\hat{a}_l$ which is 2π periodic is the Fourier transform of a_l. The sequence $a_1, \cdots, a_q$ are called wavelet frame masks, or the high pass filters of the system, and the refinement mask a_0 is called low pass filter. The unitary extension principle (UEP) of [27] asserts that the system $X(\Psi)$ generated by a finite set Ψ forms a tight frame in $L_2(\mathbb{R})$ provided that the masks $a_0, a_1, \cdots, a_q$ are finitely supported and their Fourier series satisfy

$$\sum_{l=0}^{q} |\hat{a}_l(\xi)|^2 = 1 \quad \text{and} \quad \sum_{l=0}^{q} \hat{a}_l(\xi)\overline{\hat{a}_l(\xi+\nu)} = 0,$$

for all $\nu \in \{0, \pi\}\backslash\{0\}$ and $\xi \in [-\pi, \pi]$, the framelets we adopt in this paper are constructed from piecewise linear B-spline first given in [27]. The refinement mask is $\hat{a}_0(\xi) = \cos^2(\xi/2)$, whose corresponding low pass filter is $\hat{a}_0 = \frac{1}{4}[1, 2, 1]$. The two framelet masks are $\hat{a}_1(\xi) = -\frac{\sqrt{2}i}{2}\sin^2(\xi/2)$ and $\hat{a}_2(\xi) = \sin^2(\xi/2)$, whose corresponding low pass filters are $\hat{a}_1 = \frac{\sqrt{2}}{4}[1, 0, -1]$ and $\hat{a}_2 = \frac{1}{4}[-1, 2, -1]$, respectively. We can see that the masks a_1 and a_2 correspond to the first order and second order difference operators respectively up to a scaling. The associated refinable function and framelets are given in Fig.1.

The numerical computation of the wavelet framelet transform is done by using the WF decomposition algorithm given in [28]. We conduct the decomposition algorithm without downsampling by means of refinement and framelet masks. We denote the fast framelet transform as W and the inverse framelet

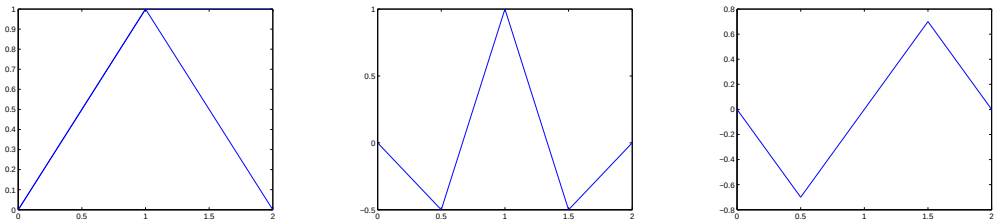

(a) ϕ (b) ψ_1 (c) ψ_2

Figure 1: Piecewise linear framelets.

transform as W^T, which is the adjoint operator of W. The frame coefficients of u can be computed by $x = Wu$, and we will have the perfect reconstruction formula $u = W^T x$, i.e., $u = W^T W u$. Hence W is a tight frame if and only if $W^T W = I$, where I is the identity matrix. Unlike the orthonormal case, we emphasize that $WW^T \neq I$ in general.

3 Numerical algorithm

3.1 Alternating direction method

The ADMM is an improved variant of the classical augmented Lagrangian method [30, 31] for solving linearly constrained convex programming problems

$$\min_{x_1,x_2} \quad \mathcal{T}_1(x_1) + \mathcal{T}_2(x_2) \quad s.t. \quad A_1x_1 + A_2x_2 = d, \quad x_i \in \Omega_i, \quad i = 1,2 \qquad (9)$$

where $\mathcal{T}_i : \Omega_i \to \mathbb{R}$ $(i = 1, 2)$, are convex functions, $A_i \in \mathbb{R}^{m\times n_i}$ $(i = 1, 2)$, and $d \in \mathbb{R}^m$, $\Omega_i, \quad i = 1, 2$ are two given closed convex sets.

An alternating minimization method was applied to the augmented Lagrangian function of (9):

$$\tilde{L}(x_1, x_2, \rho) = \mathcal{T}_1(x_1)+\mathcal{T}_2(x_2)-\rho^T(A_1x_1+A_2x_2-d)+\frac{\tau}{2}\|A_1x_1+A_2x_2-d\|_2^2, \quad (10)$$

where $\rho \in \mathbb{R}^m$ is the Lagrange multiplier and τ is a penalty parameter, which results in the following iterative scheme

$$\begin{cases} x_1^{k+1} = \arg\min_{x_1} \tilde{L}(x_1, x_2^k, \rho^k), \\ x_2^{k+1} = \arg\min_{x_2} \tilde{L}(x_1^{k+1}, x_2, \rho^k), \\ \rho^{k+1} = \rho^k - \tau(A_1x_1^{k+1} + A_2x_2^{k+1} - d). \end{cases} \qquad (11)$$

Let (x_1^*, x_2^*, ρ^*) be an saddle point of the Lagrangian function (10), then $(x_1^*, x_2^*, \rho^*) \in \Omega_1 \times \Omega_2 \times \mathbb{R}$ and it satisfies [32]

$$\begin{cases} \mathcal{T}_1(x_1) - \mathcal{T}_1(x_1^*) + (x_1 - x_1^*)^T (A_1^T(\tau(A_1x_1 + A_2x_2 - d) - \rho^*) \geq 0, \\ \mathcal{T}_2(x_2) - \mathcal{T}_2(x_2^*) + (x_2 - x_2^*)^T (A_2^T(\tau(A_1x_1 + A_2x_2 - d) - \rho^*) \geq 0, \\ (\rho - \rho^*)^T (A_1x_1 + A_2x_2 - d) \geq 0. \end{cases}$$

The authors in [32] show the convergence of the ADMM and its variant, and as a special case of the result in Theorem 1 of [32],

$$\left\| \begin{array}{c} A_2(x_2^{k+1} - x_2^*) \\ \frac{1}{\tau}(\rho^{k+1} - \rho^*) \end{array} \right\|_2^2 \leq \left\| \begin{array}{c} A_2(x_2^{k} - x_2^*) \\ \frac{1}{\tau}(\rho^{k} - \rho^*) \end{array} \right\|_2^2 - \left\| \begin{array}{c} A_2(x_2^{k+1} - x_2^k) \\ \frac{1}{\tau}(\rho^{k+1} - \rho^k) \end{array} \right\|_2^2.$$

Then by Theorem 3 in [32], $\lim_{k\to\infty}\rho^k = \rho^*$ and $\lim_{k\to\infty}A_2x_2^k = A_2x_2^*$. If matrices A_1 and A_2 have full column rank, we will get that $\lim_{k\to\infty}x_1^k = x_1^*$ and $\lim_{k\to\infty}x_2^k = x_2^*$.

Note that the two terms added to $\mathcal{T}_1(x_1) + \mathcal{T}_2(x_2)$ in (10) can be written as a single quadratic term, then we get the following alternative form of (11)

$$\begin{cases} x_1^{k+1} = \arg\min_{x_1} \mathcal{T}_1(x_1) + \frac{\tau}{2}\|A_1x_1 + A_2x_2^k - d - \bar{\rho}^k\|_2^2, \\ x_2^{k+1} = \arg\min_{x_2} \mathcal{T}_2(x_2) + \frac{\tau}{2}\|A_1x_1^{k+1} + A_2x_2 - d - \bar{\rho}^k\|_2^2, \\ \bar{\rho}^{k+1} = \bar{\rho}^k - (A_1x_1^{k+1} + A_2x_2^{k+1} - d), \end{cases} \tag{12}$$

where $\bar{\rho}^k = \frac{\rho^k}{\tau}$ and ρ^k is determined in (11).

The equivalence of (11) and (12) implies that instead (10), we can consider the augmented Lagrange function

$$\tilde{L}(x_1, x_2, \rho) = \mathcal{T}_1(x_1) + +\mathcal{T}_2(x_2) + \frac{\tau}{2}\|A_1x_1 + A_2x_2 - \frac{1}{\tau}\rho\|_2^2, \tag{13}$$

where $\rho \in \mathbb{R}^m$ is the Lagrange multiplier and τ is a penalty parameter,

3.2 Proposed algorithm

Here we discuss the details of the algorithm to solve the hybrid model (6). The proposed algorithm is an application of the ADMM. By introducing three auxiliary variables x, y, z, we reformulate the model (6) as the following constrained optimization problem

$$\min_{u,x,y,z} \sum_{i,j=1}^{n} (x+b)_{i,j} - f_{i,j}\log(x+b)_{i,j} + \alpha\|y\|_1 + \beta\|z\|_1, \tag{14}$$

$$s.t. \quad Ku = x, Wu = y, \nabla u = z.$$

It is not difficult to see that the problem (14) is a special case of the problem (9) with the following specifications,

$$A_1 = \begin{pmatrix} K \\ W \\ \nabla \end{pmatrix}, A_2 = \begin{pmatrix} -I & 0 & 0 \\ 0 & -I & 0 \\ 0 & 0 & -I \end{pmatrix}, x_1 = u, x_2 = \begin{pmatrix} x \\ y \\ z \end{pmatrix}, d = \begin{pmatrix} 0 \\ 0 \\ 0 \end{pmatrix}.$$

The resulting augmented Lagrangian function is

$$\begin{aligned} L(u,x,y,z) = \sum_{i,j=1}^{n} (x+b)_{i,j} - f_{i,j}\log(x+b)_{i,j} + \frac{\sigma_1}{2}\|Ku - x + \frac{\lambda_1}{\sigma_1}\|_2^2 + \alpha\|y\|_1 \\ + \frac{\sigma_2}{2}\|Wu - y + \frac{\lambda_2}{\sigma_2}\|_2^2 + \beta\|z\|_1 + \frac{\sigma_3}{2}\|\nabla u - z + \frac{\lambda_3}{\sigma_3}\|_2^2, \end{aligned}$$

where λ_1, λ_2 and λ_3 are the vectors corresponding to the Lagrange multipliers to the linear constraints, and σ_1, σ_2 and σ_3 are the penalty parameters of the ADMM to control the speed of the convergence; see, for instance, [33]. We denote $d_1 = \frac{\lambda_1}{\sigma_1}$, $d_2 = \frac{\lambda_2}{\sigma_2}$ and $d_3 = \frac{\lambda_3}{\sigma_3}$, then the above equation can be rewritten as

$$\begin{aligned} L(u,x,y,z) = \sum_{i,j=1}^{n} (x+b)_{i,j} - f_{i,j}\log(x+b)_{i,j} + \frac{\sigma_1}{2}\|Ku - x + d_1\|_2^2 + \alpha\|y\|_1 \\ + \frac{\sigma_2}{2}\|Wu - y + d_2\|_2^2 + \beta\|z\|_1 + \frac{\sigma_3}{2}\|\nabla u - z + d_3\|_2^2. \end{aligned} \tag{15}$$

Since the variables u, x, y and z are decoupled, this allows us to solve them more easily on their corresponding subproblems in the ADMM. We now investigate these subproblems one by one for the Poisson noise removal problem.

Firstly, we solve for the variable u in the subproblem. This subproblem corresponds to the following optimization problem

$$u^{k+1} = \arg\min_u \frac{\sigma_1}{2}\|Ku - x^k + d_1^k\|_2^2 + \frac{\sigma_2}{2}\|Wu - y^k + d_2^k\|_2^2 + \frac{\sigma_3}{2}\|\nabla u - z^k + d_3^k\|_2^2,$$

The minimizer can be obtained by equivalently solving a linear system

$$(\sigma_1 K^T K + \sigma_2 I + \sigma_3 \nabla^T \nabla)u^{k+1} = \sigma_1 K^T(x^k - d_1^k) + \sigma_2 W^T(y^k - d_2^k) + \sigma_3 \nabla^T(z^k - d_3^k), \tag{16}$$

where ∇^T represents the conjugate operator of ∇, and we have used $W^T W = I$. Under the periodic boundary conditions, the matrices K and ∇ have block

circulant with circulant blocks (BCCB) structure, so the above linear system can be efficiently solved by using FFTs. Denoting $\mathcal{F}(u)$ as the fast Fourier transform of u, We can write

$$u^{k+1} = \mathcal{F}^{-1}(\eta),$$

where

$$\eta = \frac{\mathcal{F}(\sigma_1 K^T(x^k - d_1^k) + \sigma_2 W^T(y^k - d_2^k) + \sigma_3 \nabla^T(z^k - d_3^k))}{\mathcal{F}(\sigma_1 K^T K + \sigma_2 I + \sigma_3 \nabla^T \nabla)}. \tag{17}$$

The minimization of L with respect to x is expressed as the following simple form

$$x^{k+1} = \arg\min_x \sum_{i,j=1}^{n} (x+b)_{i,j} - f_{i,j}\log(x+b)_{i,j} + \frac{\sigma_1}{2}\|Ku^{k+1} - x + d_1^k\|_2^2.$$

The corresponding solution can be obtained

$$x^{k+1} = \frac{1}{2}\left((Ku^{k+1} + b + d_1^k - \frac{1}{\sigma_1}) + \sqrt{(Ku^{k+1} + b + d_1^k - \frac{1}{\sigma_1})^2 + 4\frac{f^T}{\sigma_1}}\right) - b. \tag{18}$$

The minimization of L with respect to y is expressed as the following simple form

$$y^{k+1} = \arg\min_y \alpha\|y\|_1 + \frac{\sigma_2}{2}\|Wu^{k+1} - y + d_2^k\|_2^2.$$

The corresponding solution can be obtained

$$y^{k+1} = S_{soft}((Wu^{k+1} + d_2^k)_i, \frac{\alpha}{\sigma_2}) \tag{19}$$

where

$$S_{soft}(x, \delta) = \begin{cases} 0, & |x| < \delta, \\ x - \delta \text{sign}(x), & |x| \geq \delta. \end{cases}$$

The minimization of L with respect to z is expressed as the following simple form

$$z^{k+1} = \arg\min_z \beta\|z\|_1 + \frac{\sigma_3}{2}\|\nabla u^{k+1} - z + d_3^k\|_2^2.$$

The corresponding solution can be obtained

$$z^{k+1} = S_{soft}((\nabla u^{k+1} + d_3^k)_i, \frac{\beta}{\sigma_3}). \tag{20}$$

On the other hand, the updating scheme of the Lagrangian multipliers can be rewritten specifically as

$$\begin{aligned} d_1^{k+1} &= d_1^k + (Ku^{k+1} - x^{k+1}), \\ d_2^{k+1} &= d_2^k + (Wu^{k+1} - y^{k+1}), \\ d_3^{k+1} &= d_3^k + (\nabla u^{k+1} - z^{k+1}). \end{aligned} \tag{21}$$

The resulting algorithm based ADMM is summarized as Algorithm 1.

Algorithm 1 ADMM for the image restoration problem (6)

Initialization: $\epsilon_{tol}, MaxIter, u^0 = f, x^0 = 0, y^0 = Wf, z^0 = \nabla f, \sigma_1, \sigma_2, \sigma_3, d_i^0 = 0$ for $i = 1, 2, 3, k = 0, const = 1$.

Iteration:

while (const)

compute u: $u^{k+1} = \mathcal{F}^{-1}(\eta), \eta$ is defined in (17);

compute x: $x^{k+1} = \frac{1}{2}\Bigg((Ku^{k+1} + b + d_1^k - \frac{1}{\sigma_1}) + \sqrt{(Ku^{k+1} + b + d_1^k - \frac{1}{\sigma_1})^2 + 4\frac{f^T}{\sigma_1}} \Bigg) - b;$

compute y: $y^{k+1} = S_{soft}((Wu^{k+1} + d_2^k)_i, \frac{\alpha}{\sigma_2})$;

compute z: $z^{k+1} = S_{soft}((\nabla u^{k+1} + d_3^k)_i, \frac{\beta}{\sigma_3})$;

update d_1: $d_1^{k+1} = d_1^k + (Ku^{k+1} - x^{k+1})$;

update d_2: $d_2^{k+1} = d_2^k + (Wu^{k+1} - y^{k+1})$;

update d_3: $d_3^{k+1} = d_3^k + (\nabla u^{k+1} - z^{k+1})$;

$const = \|u^{k+1} - u^k\|_2 / \|u^k\|_2 > \epsilon_{tol}$ or $k < MaxIter$;

$k = k + 1$;

4 Numerical experiments

In this section, we conduct several numerical experiments to illustrate the performance of the proposed hybrid model. All the experiments were performed using MATLAB 7.7.0 on a computer equipped with an Intel (R) Core (TM) 2.60 GHz processor, with 4.00 GB of RAM, and running Windows XP.

We compare our method with PIDAL algorithm proposed in [34]), which can be regarded as special cases of Algorithm 1. If we choose $\beta = 0$ or $\alpha = 0$ in Algorithm 1, we obtain PIDAL$_{TV}$ algorithm (only TV regularizer) and PIDAL$_{FA}$ algorithm (only tight frame regularizer) respectively.

The quality of the restored images is measured by Peak-signal-to-noise ratio (PSNR), Structural similarity index (SSIM) and the Relative error (ReErr). They are defined as follows:

$$\text{PSNR} = 20\log_{10}\frac{255}{\frac{1}{mn}\|u - f^*\|_2},$$

$$\text{SSIM} = \frac{(2\mu_f^*\mu_u + C_1)(2\sigma_{f^*u} + C_2)}{(\mu_{f^*}^2 + \mu_u^2 + C_1)(\sigma_{f^*}^2 + \sigma_u^2 + C_2)}.$$

$$\text{ReErr} = \frac{\|u-f^*\|_2}{\|f^*\|_2},$$

where f^* is the original image, and u is the restored image. μ_{f^*} and μ_u are averages of f^* and u respectively, σ_{f^*} and σ_u are the variance of f^* and u respectively, σ_{f^*u} is the covariance of f^* and u and the positive constants C_1 and C_2 can be thought of as stabilizing constants for near-zero denominator values. In general, a high PSNR-value or a small ReErr-value indicates the restoration is more accurate. However, we know that the PSNR-value or a small ReErr-value are not always in agreement with visual perception. The SSIM index is a well-known quality metric used to measure the similarity between two images. The SSIM map is whiter, the restored image is closer to the clean image.

We use the stopping criterion when the maximum number of allowed outer iterations $MaxIter$ has been carried out or the relative differences between consecutive iterates $u^1, u^2, u^3, \cdots$ satisfy

$$\frac{\|u^{k+1} - u^k\|_2}{\|u^{k+1}\|_2} < \epsilon_{tol}.$$

In this paper, we set $MaxIter = 100$ and $\epsilon_{tol} = 10^{-4}$.

It is known that the quality of the restored image is highly depended on the regularization parameters. In order to have fair comparisons for the three methods, we use the best regularization parameters such that the optimal PSNR values are achieved. Regarding the penalty parameters σ's in Algorithm 1, theoretically any positive values of σ_1, σ_2 and σ_3 ensure the convergence of the ADMM [32]. However, the penalty paremeter does influence the speed of the algorithms [34]. In numerical experiments, we test some values of these parameters and pick a optimal value with satisfactory results.

(a) Lena

(b) House

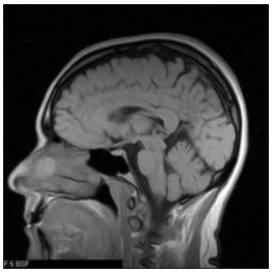

(c) Brain

(d) Cameraman

(e) Butterfly

Figure 2: Original images.

Table 1: Output of the experiments

Images	Blur	PSNR			SSIM		
		TV	Frame	Proposed	TV	Frame	Proposed
Lena	Defocus	24.790	25.103	**25.242**	0.7098	0.7338	**0.7331**
	Motion	27.477	27.403	**27.977**	0.8008	0.8016	**0.8309**
	Gauss	26.340	26.519	**26.737**	0.7687	0.7888	**0.7919**
House	Defocus	26.140	26.599	**26.697**	0.7228	0.7268	**0.7301**
	Motion	28.741	28.666	**29.344**	0.8074	0.7698	**0.8158**
	Gauss	27.231	27.527	**27.852**	0.7767	0.7806	**0.7912**
Brain	Defocus	27.219	27.553	**27.738**	0.7957	0.7941	**0.7980**
	Motion	29.900	29.872	**30.786**	0.8705	0.8662	**0.8831**
	Gauss	29.595	30.426	**30.529**	0.8661	0.8704	**0.8780**
Butterfly	Defocus	25.995	26.175	**26.209**	0.8327	0.8380	**0.8417**
	Motion	27.914	26.006	**28.191**	0.9023	0.8764	**0.9101**
	Gauss	27.406	27.688	**27.746**	0.8934	0.9010	**0.9020**
Cameraman	Defocus	23.384	23.375	**23.583**	0.6949	0.6891	**0.7238**
	Motion	25.288	25.438	**25.715**	0.7550	0.7364	**0.7910**
	Gauss	24.223	24.049	**24.402**	0.7565	0.7611	**0.7630**

The test images are shown in Figure 2. In order to simulate the degraded operation in the tests, we generate the blurred and noisy images by blurring the true images with the given different point spread functions and additionally contaminate it by Poisson noise, which is implemented by applying the Matlab routine *poissrnd*. For each image, we consider three different blurs: the out-of-focus blur proposed in [35], the Gauss blur function $psfGauss$ proposed in [36] and the linear motion blur in [37]. In this paper, we choose the out-of-focus blur with radius 9 which is generated by MATLAB function $ones(9,9)/18$, the Gauss blur with $dim = 7$ and $s = 2$ which is generated by MATLAB function $psfGauss(7,2)$, and the linear motion blur with $r = 7$ and $\theta = 45$ which is generated by MATLAB function $fspecial('motion', 7, 45)$.

In Figures 3 and 4, we show the restoration results when the tight frame method, the total variation method and the hybrid method are applied to the image restoration problem for the motion blur. From the visual quality of restored images, the proposed method is competitive with the other two methods. For showing the effectiveness of our method, we give the SSIM maps of the restored images with respect to the original images in Figures 3(f)-(h) and 4(f)-(h). From these images, we can see that the SSIM map of the restored image obtained by our method is slightly whiter than those by the other methods, i.e., our method can get better restoration results.

In Figure 5, we plot the convergence results about PSNR versus iteration for different methods. We observe that the proposed methods is convergent and get higher PSNR values than others.

In Figure 6, the original image, the degraded image and the restoration images of the Lena image by three methods are exhibited. Visually, the proposed method is better than the other methods since the image recovered by the proposed method preserves more details and looks more natural.

For a better visual comparison, we have enlarged some details of the three restored images in Figures 7 and 8. As can be seen in the zoomed parts (the part shown as the white rectangle in Figure 6(a)), our method has less staircase effects and makes a good compromise between edge preserving and smoothing.

In Table 1, the PSNR and SSIM values of three methods are presented, which shows that our method yields a better restoration result. Therefore, we conclude that the proposed method performs better than the tight frame method and the total variation method.

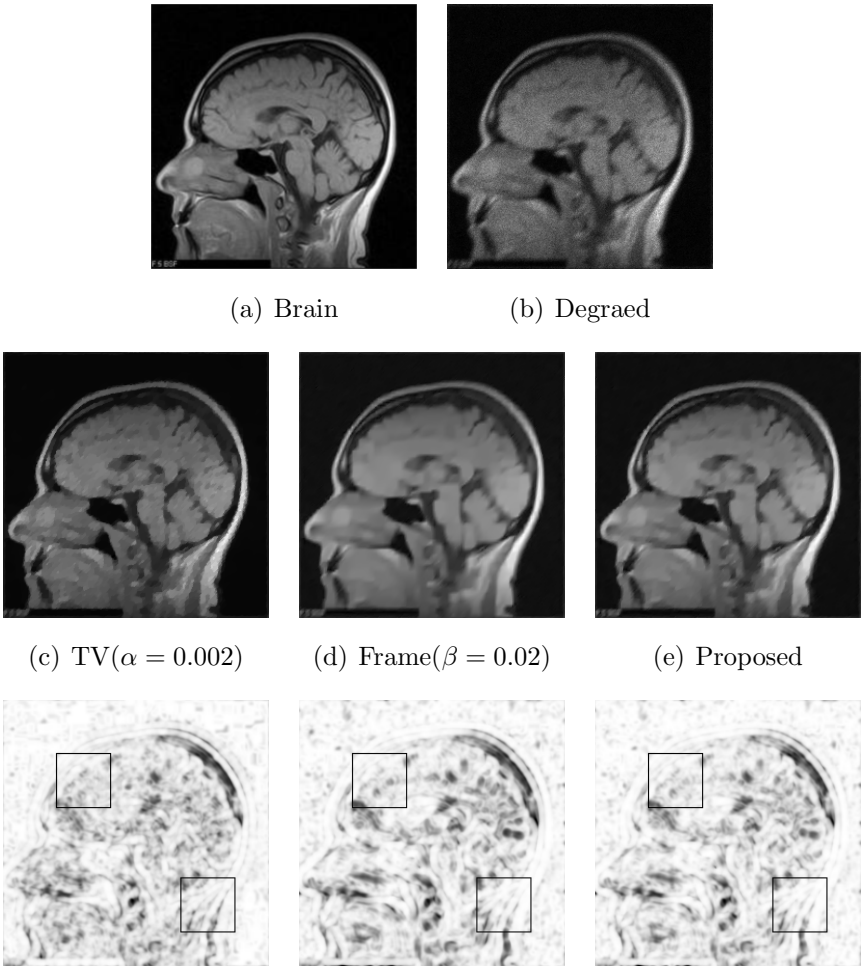

(a) Brain (b) Degraed

(c) TV($\alpha = 0.002$) (d) Frame($\beta = 0.02$) (e) Proposed

(f) TV (g) Frame (h) Proposed

Figure 3: Restoration results for the image "Brain" under the Motion blur($\alpha = 0.01, \beta = 0.008, \sigma_1 = \sigma_2 = \sigma_3 = 0.002$).

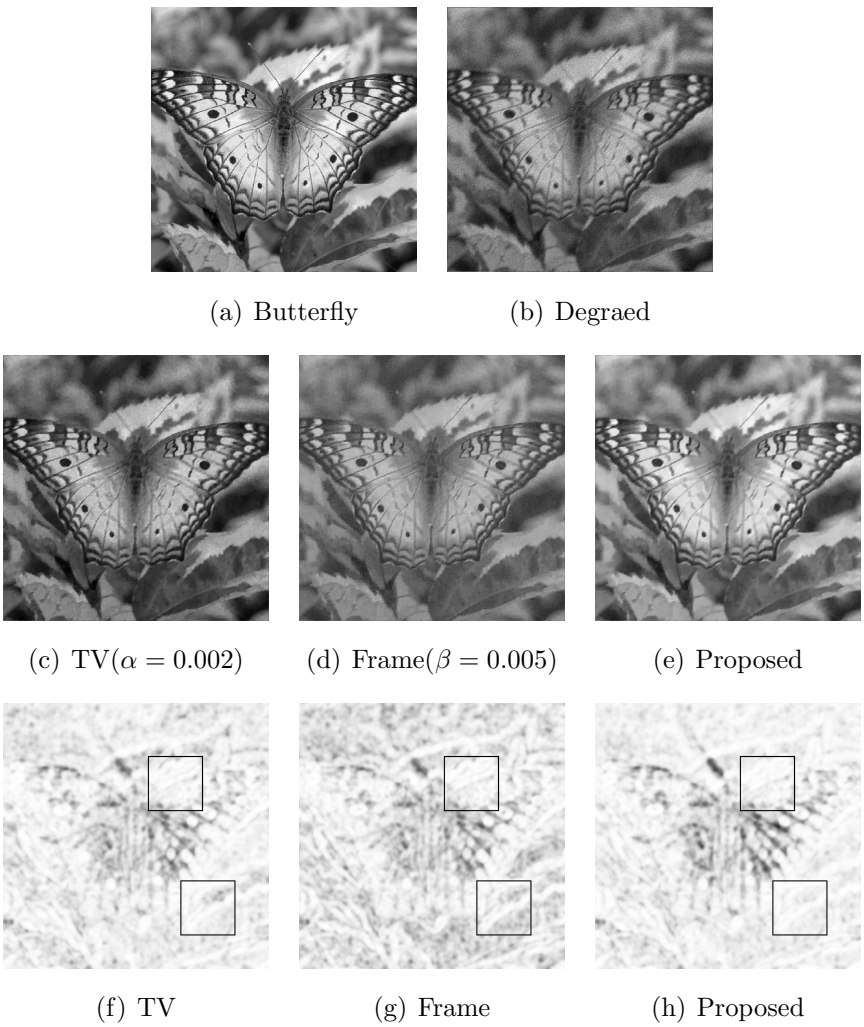

(a) Butterfly (b) Degraed

(c) TV($\alpha = 0.002$) (d) Frame($\beta = 0.005$) (e) Proposed

(f) TV (g) Frame (h) Proposed

Figure 4: Restoration results for the image "Butterfly" under the Motion blur($\alpha = 0.005, \beta = 0.01, \sigma_1 = \sigma_2 = \sigma_3 = 0.001$).

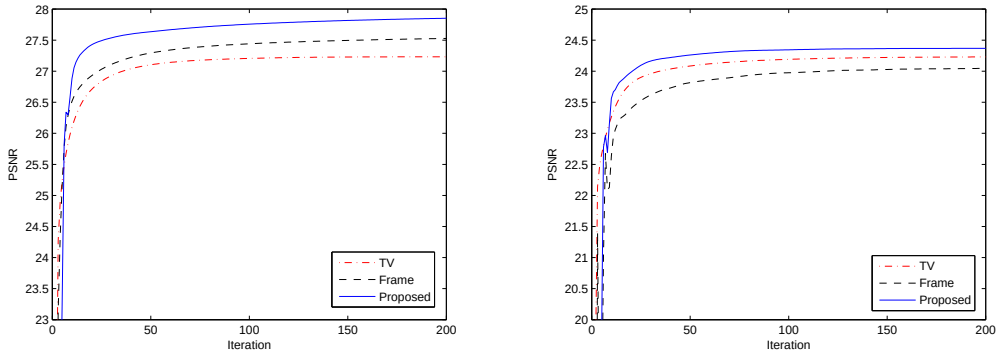

(a) House (b) Cameraman

Figure 5: Convergence results for the images "House" and "Cameraman" under the Gauss blur.

(a) Lena (b) Degraded

(c) TV($\alpha = 0.002$) (d) Frame($\beta = 0.008$) (e) proposed

Figure 6: Restoration results for the image "Lena" under the motion blur($\alpha = 0.005, \beta = 0.01, \sigma_1 = \sigma_2 = \sigma_3 = 0.005$).

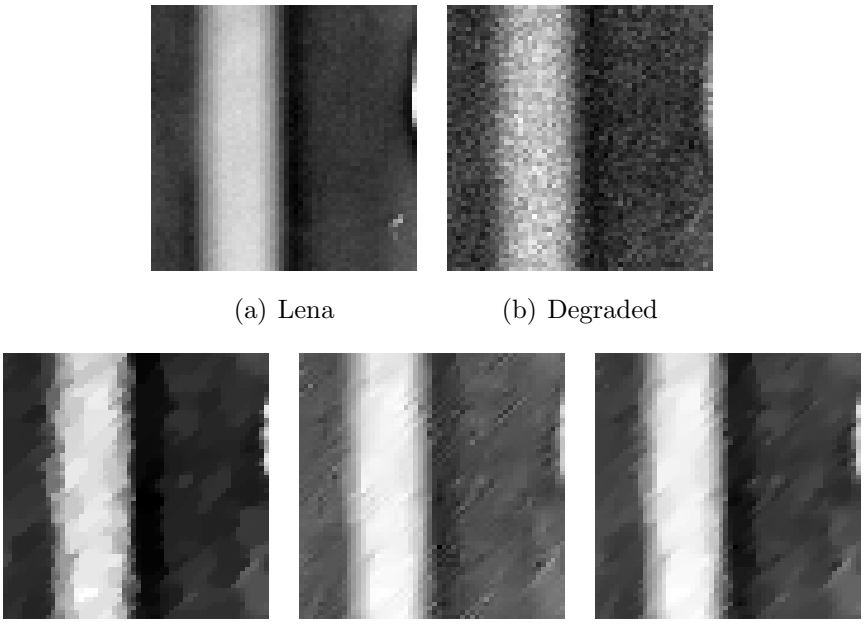

(a) Lena (b) Degraded

(c) TV (d) Frame (e) proposed

Figure 7: Restoration results for the image "Lena" under the motion blur.

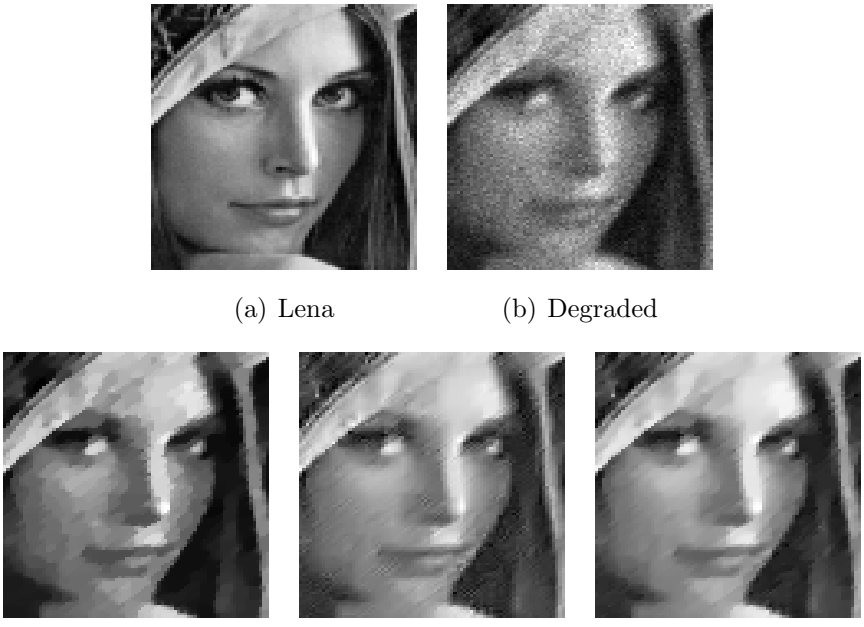

(a) Lena (b) Degraded

(c) TV (d) Frame (e) proposed

Figure 8: Restoration results for the image "Lena" under the motion blur.

5 Conclusion

In this paper, we consider the alternating direction method for restoring blurred images corrupted by Poisson noise. The proposed method combines advantages of the wavelet tight frame and TV. The proposed model utilizes the characteristic of wavelet frame in preserving image details and suppressing the staircase effect. The numerical experiments show that the proposed method outperforms some existimg restoration methods in terms of the PSNR, and SSIM map for the Poisson noise removal problem.

References

[1] J.-L.Starck and F. Murtagh, Astronomical Image and Data Analysis, *New York: Springer-Verlag*, **57**(57), (2002), 8-14.

[2] P. Sarder and A. Nehorai, Deconvolution method for 3-D fluorescence microscopy images, *IEEE Signal Processing Magazine*, **23**(3), (2006), 32-45.

[3] A. Foi, S. Alenius, M. Trimeche, V. Katkovnik and K. Egiazarian, A spatially adaptive Poissonian image deblurring, *IEEE International Conference on Image Processing*, **1**, (2005), 925-928.

[4] N. Dey, L. Blanc-Feraud, C. Zimmer, P. Roux, Z. Kam, J. Olivo-Marin and J. Zerubia, Richardson-Lucy algorithm with TV regularization for 3D confocal microscope deconvolution, *Microscopy Research Technique*, **69**(4), (2006), 260-266.

[5] L. B. Lucy, An iterative technique for rectification of observed distributions, *The Astronomical Journal*, **79**(6), (1974), 745-765.

[6] W. H. Richardson, Bayesian-based iterative method of image restoration, *Journal of Optical Society of America*, **62**(1), (1972), 55-59.

[7] H. H. Barrett and K. J. Meyers, *Foundations of Image Science*, New York: Wiley, 2003, 1047-1048.

[8] F. Natterer and F. Wübbeling, Mathematical Methods in image Reconstruction, *Society for Industrial and Applied Mathematics*, **29**(1), (2001), 118-123.

[9] A. Staglianò, P. Boccacci and M. Bertero, Analysis of an approximate model for Poisson data reconstruction and a related discrepancy principle, *Inverse Problems*, **27**(12), (2011), 1061-1063.

[10] C. R. Vogel, *Computational Methods for Inverse Problems*, SIAM, Philadelphia, 2002.

[11] A. Tikhonov and V. Arsenin, *Solution of Ill-Posed Problems*, Winston, Washington, D.C., 1977.

[12] J. M. Bardsley and C. R. Vogel, A nonnegatively constrained convex programming method for image reconstruction, *SIAM Journal on Scientific Computing*, **25**(4), (2004), 1326-1343.

[13] J. M. Bardsley and N. Laobeula, Tikhonov regularized Poisson likelihood estimation: theoretical justification and a computational methd, *Inverse Problems in Science and Engineering*, **16**(2), (2008), 199-215.

[14] L. Rudin, S. Osher and E. Fatemi, Nonlinear total variation based noise removal algorithms, *Physica D*, **60**(1), (1992), 259-268.

[15] L. Rudin and S. Osher, Total variation based image restoration with free local constraints, *IEEE International Conference on Image Processing*, **1**, (1994), 31-35.

[16] A. Sawatzky, C. Brune, F. Wubbeling, T. Kosters, K. Schafers and M. Burger, Accurate EM-TV algorithm in PET with low SNR, *IEEE Nuclear Science Symposium Conference Record*, (2008), 5133-5137.

[17] M. A. T. Figueiredo and J. M. Bioucas-Dias, Restoration of Poissonian images using alternating direction optimization, *IEEE Transactions Image Processing*, **19**(2), (2010), 3133-3145.

[18] C. Brune, A. Sawatzky, M. Burger, Bregman-EM-TV Methods with Application to Optical Nanoscopy, *Proceedings of the 2nd International Conference on Scale Space and Variational Methods in Computer Vision, Springer, Berlin*, **5567**, (2009), 235-246.

[19] Y. Meyer, Oscillating patterns in Image Processing and Nonlinear Evolution Equations, *the fifteenth Dean Jacqueline B. Lewis memorial lectures*, **22**, (2001), 71-117.

[20] D. Q. Chen and L. Z. Cheng, Deconvoling Poissonian images by a novel hybrid variational model, *Journal of Visual Communication and Image* , **22**, (2011), 643-652.

[21] D. Q. Chen, Regularized Generalized Inverse Accelerating Linearized Alternating Minimization Algorithm for Frame-based Poissonian Image Deblurring, *SIAM Journal of Imaging Sciences*, **7**(1), (2014), 716-739.

[22] S. Mallat, *A Wavelet Tour of Signal Processing*, second ed., Academic Press, 1999.

[23] T. Chan, A. Marquina and P. Mulet, High-order total variation-based image restoration, *SIAM Journal on Scientific Computing*, **22**(2), (2000), 503-516.

[24] A. Chai, Z. Shen, Deconvolution: a wavelet frame approach, *Numerische Mathematik*, **106**(4), (2007), 529-587.

[25] J. Chai, Z. Shen, Framelet based deconvolution, *Journal of Computational Mathematics*, **28**(3), (2010), 289-308.

[26] I. Daubechies, Ten Lectures on Wavelets, *SIAM, Philadelphia*, **61**, 1992.

[27] A. Ron and Z. Shen, Affine Systems in $L_2(\mathbb{R})$: The Analysis of the Analysis Operator, *Journal of Functional Analysis*, **148**(2), (1997), 408-447.

[28] I. Daubechies, B. Han, A. Ron and Z. Shen, Framelets: MRA-based constructions of wavelet frames, *Applied and Computational Harmonic Analysis*, **14**(1), (2003), 1-46.

[29] J. F. Cai, B. Dong, S. Osher and Z. Shen. Image restoration: Total variation, wavelet frames, and beyond, *Journal of the American Mathematical*, **25**(4), (2012), 1033-1089.

[30] M. R. Hestenes, Multiplier and gradient methods, *Journal of Optimization Theorey and Applications*, **4**(5), (1969), 303-320.

[31] M. J. D. Powell, A method for nonlinear constraints in minimization problems, *Optimization*, **5**(6), (1969), 283-298.

[32] B. S. He and H. Yang, Some convergence properties of a method of multipliers for linearly constrained monotone variational inequalities, *Operations Research Letters*, **23**(3-5), (1998), 151-161.

[33] M. K. Ng, P. Weiss and X. Yuan, Solving constrained total-variation image restoration and reconstruction problems via alternating direction methods, *SIAM Journal on Scientific Computing*, **32**(5), (2010), 2710-2736.

[34] M. Figueiredo and J. Bioucas-Dias, Restoration of Poissonian images using alternating direction optimization, *IEEE Transactions on Image Processing*, **19**(12), (2010), 3133-3145.

[35] Y. M. Huang, M. K. Ng and Y. M. Wen, A fast total variation minimization method for image restoration, *SIAM Journal of Multiscale Modeling Simulation*, **7**(2), (2008), 774-795.

[36] J. G. Nagy, K. Palmer and L. Perrone, Iterative methods for image deblurring: a matlab object-oriented approach, *Numerical Algorithms*, **36**(1), (2004), 73-93.

[37] F. Li and T. Zeng, Image restoration via tight frame regularization and local constraints, Journal of Scientific Computing, **57**(2), (2013), 349-371.